GEOLOGY | THE GEOLOGICAL SOCIETY OF AMERICA®

https://doi.org/10.1130/G50258.1

Manuscript received 28 March 2022
Revised manuscript received 13 July 2022
Manuscript accepted 15 July 2022

Published online 20 October 2022

Fault surface morphology as an indicator for earthquake nucleation potential

Agathe M. Eijsink[1], James D. Kirkpatrick[2], François Renard[3,4] and Matt J. Ikari[1]
[1]Center for Marine Environmental Sciences (MARUM), University of Bremen, 28359 Bremen, Germany
[2]Department of Earth & Planetary Sciences, McGill University, Montréal, Québec H3A 0E8, Canada
[3]Njord Centre, Departments of Geosciences and Physics, University of Oslo, P.O. Box 1048, Blindern, 0316 Oslo, Norway
[4]Institut des Sciences de la Terre (ISTerre), CNRS, University Grenoble Alpes, 38000 Grenoble, France

ABSTRACT

Laboratory measurements can determine the potential for geologic materials to generate unstable (seismic) slip, but a direct relation between sliding behavior in the laboratory and physical characteristics observable in the field is lacking, especially for the phyllosilicate-rich gouges that are widely observed in natural faults. We integrated laboratory friction experiments with surface topography microscopy and demonstrated a quantitative correlation between frictional slip behavior and fault surface morphology of centimeter-scale samples. Our results show that striated, smooth fault surfaces were formed in experiments that exhibited stable sliding, whereas potentially unstable sliding was associated with rougher, isotropic fault surfaces. We interpret that frictional stability and fault surface morphology are linked via the evolution of asperity contacts on localized slip surfaces. If fault surface roughness obeys a fractal relationship over a large range of length scales, then we infer that the morphological characteristics observed in the laboratory could indicate the earthquake nucleation potential on natural fault surfaces.

INTRODUCTION

Laboratory friction experiments have provided the basis for a theoretical framework that predicts the stability of a slipping fault via measurements of velocity-dependent frictional strength (e.g., Scholz, 1998). However, because earthquakes occur on fault surfaces that are many orders of magnitude larger than typical laboratory samples, laboratory-measured parameters have to be related to measurable quantities that can be extrapolated over a wide range of length scales. Fault surface morphology analysis is a promising tool for this extrapolation because fault roughness can be measured relatively easily and exhibits a consistent self-affine scaling across length scales ranging from the laboratory to the field (Power et al., 1987; Candela et al., 2012).

Fault surfaces, as well as other frictional slip surfaces formed by landslides (Shuzui, 2001) or glaciers (Kamb, 1970), commonly contain structures such as slickensides or grooves that are oriented parallel to the slip direction (Doblas, 1998) (Fig. 1). These features combine to define a surface topography characteristic of natural fault outcrops (Power et al., 1987; Bistacchi et al., 2011; Candela et al., 2012; Brodsky et al., 2016). A recent study by Kirkpatrick et al. (2020) showed that the topography of fault surfaces at depths of several kilometers can be measured at the scale of tens of kilometers and might control earthquake nucleation. Currently, the frictional properties of such inaccessible faults cannot be directly measured, but they could be inferred if laboratory-measured frictional parameters can be linked to surface roughness parameters.

Previous laboratory friction experiments confirmed a close connection between roughness and frictional behavior (Dieterich and Kilgore, 1994). Artificially varying the surface roughness as a starting condition affects frictional strength (Biegel et al., 1992), slip stability (Harbord et al., 2017), and critical slip distance (Okubo and Dieterich, 1984). Additionally, the final roughness is controlled by the starting roughness (Badt et al., 2016), and differences in deformation mechanisms cause variations in fault surface morphology (Sagy et al., 2017).

We measured the surface roughness evolution on experimental faults composed of quartz or shale as a quantitative microstructural study and established a relationship between slip surface roughness and velocity-dependent friction parameters. In contrast to earlier work, the initial fault surface morphology developed spontaneously by shearing initially undeformed (remolded) samples. In particular, the shale represents phyllosilicate-rich faults, which have not been previously studied in surface roughness experiments but are commonly observed to localize slip in natural faults (e.g., Collettini et al., 2009).

METHODS

Using a single direct shear device (see the Supplemental Material[1] for methods, and Figures S1–S3 therein), we performed (1) velocity-stepping experiments, where sliding velocity was alternated between 1 and 10 μm/s every millimeter of displacement in the range 2–10 mm, and (2) shearing experiments at a constant velocity of 10 μm/s to a total displacement of 2–10 mm. The direct shear geometry forces the samples to fail along a localized shear plane, which then acts as the locus of subsequent slip, generating a slip surface analogous to localized deformation planes exposed in natural faults. Roughness of the slip surfaces was measured from the constant velocity experiments, with the velocity-stepping experiments providing the frictional data at matching displacements. Experiments were performed on fully drained, water-saturated samples at 10 MPa effective normal stress, conditions representative for faults in the shallow crust and other frictional

[1]Supplemental Material. Supplemental figures providing background data to the manuscript, and a detailed description of the methods used. Please visit https://doi.org/10.1130/GEOL.S.20669244 to access the supplemental material, and contact editing@geosociety.org with any questions.

CITATION: Eijsink, A.M., et al., 2022, Fault surface morphology as an indicator for earthquake nucleation potential: Geology, v. XX, p. , https://doi.org/10.1130/G50258.1

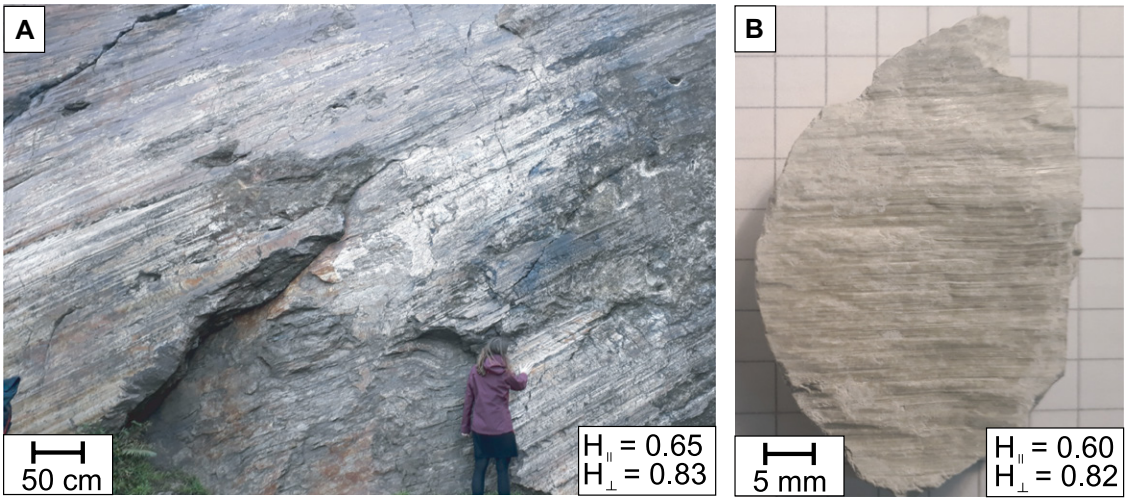

Figure 1. Fault striations on multiple scales. (A) Corona Heights fault (San Francisco, California), showing large-scale striations. Hurst exponents H and $H_{\parallel}$ (measured perpendicular and parallel to the shear direction, respectively) are from Candela et al. (2012). (B) Fault recovered in drill core from the Hikurangi margin (New Zealand), sample U1520C-5R2 (Wallace et al., 2019).

sliding processes that occur under relatively low normal stresses.

We described the velocity-dependent frictional behavior in terms of rate-and-state friction (see the Supplemental Material), where the parameter $a\text{-}b = \Delta\mu_{ss}/\Delta\ln V$ is the change in steady-state friction coefficient ($\Delta\mu_{ss}$) that occurs when changing the sliding velocity V. Positive values of $a\text{-}b$ indicate velocity-strengthening behavior, for which stable sliding is expected, whereas slip instabilities, such as earthquakes, can only nucleate when $a\text{-}b$ is negative (velocity-weakening behavior). Since this is the first study to quantitatively relate roughness development during shear with friction parameters, we tested synthetic quartz powder as a representative velocity-weakening material (Logan and Rauenzahn, 1987) and powdered Rochester shale of comparable grain size as a representative velocity-strengthening material (Saffer and Marone, 2003).

Surface roughness was measured with a confocal laser scanning microscope (CLSM), with some supplemental measurements made with a white light interferometer (WLI). We quantified surface roughness using the power spectral density (PSD) as

$$\mathrm{PSD} = C\left(\frac{1}{\lambda}\right)^{(2H+1)}, \quad (1)$$

where C is an empirical constant, λ is the wavelength, and H is the Hurst exponent (Power et al., 1987). The PSD value gives the absolute roughness of a fault surface for each wavelength. The scaling Hurst exponent, with values commonly in the range of ~0.4–1 (Candela et al., 2012; Sagy et al., 2017), shows an azimuthal dependence on striated fault surfaces (Renard et al., 2006). When $H < 1$ (self-affine), the surface becomes smoother at larger scales. We calculated the degree of anisotropy, A, as

$$A = \frac{H_{\perp} - H_{\parallel}}{H_{\perp}}, \quad (2)$$

where $H_{\perp}$ and $H_{\parallel}$ are the maximum and minimum Hurst exponents measured perpendicular and parallel to the shear direction.

STRIATIONS AND FRICTIONAL BEHAVIOR

Fault surfaces recovered from the experiments show a clear distinction between the shale and quartz samples. After displacements ≥4 mm, the shale developed smooth, striated fault surfaces (Fig. 2A), whereas the quartz faults were rougher and lacked striations (Fig. 2B). The roughness measurements confirmed these observations, showing that roughness at a reference wavelength of 1 mm decreased for the shale samples during the first few millimeters of sliding, whereas the quartz fault remained consistently rougher with a constant roughness (Fig. 2C). Furthermore, the Hurst exponents $H_{\parallel}$ and $H_{\perp}$ (Fig. S4) were both constant at ~0.4 for the quartz surfaces, resulting in a low roughness anisotropy, $A = 0 \pm 0.13$, for all displacements (Fig. 2D). The shale fault showed higher values of $H_{\parallel}$ and $H_{\perp}$ of ~0.6 and ~0.8, which are more typical of natural fault zones (Candela et al., 2012), causing the anisotropy to increase up to $A = 0.25$ with increasing displacement (Fig. 2D).

The parameter $a\text{-}b$ is negative for the nearly isotropic quartz (−0.003) and the initially isotropic shale after 2 mm displacement (−0.006). At displacements ≥4 mm, $a\text{-}b$ in the shale experiment becomes positive (0.004; Fig. 2E), correlating with the transition to anisotropic surface roughness. The difference in $a\text{-}b$ is mainly caused by differences in b, which is close to zero for the anisotropic shale and around 0.008 for the quartz and initially isotropic shale (Fig. 2F; Fig. S5), whereas a is relatively constant (0.004) for both the shale and the quartz.

Our results show a relationship between surface roughness and frictional stability parameters: striated, anisotropic fault surfaces in shale show velocity-strengthening behavior, whereas velocity-weakening friction is associated with rough, nearly isotropic fault surfaces in both sample materials. These simple systematics are consistent with previous experimental studies. In quartz, striated surfaces have been produced under hydrothermal conditions (Toy et al., 2017). Striated patches have been produced on limestone bare surfaces (Sagy et al., 2017) under conditions where there is no frictional healing (Tesei et al., 2017), a requirement for slip instabilities. Direct observations of the surface morphology of a single salt crystal showed that $a\text{-}b$ increases and slip instabilities disappear when the contact asperities evolve from initially isotropic to elongated and anisotropic (Voisin et al., 2007).

In general, $a\text{-}b$ depends on a range of factors, such as sliding velocity, normal stress, temperature, and microstructural development (Logan and Rauenzahn, 1987; Saffer and Marone, 2003; den Hartog and Spiers, 2014). In our experiments, the experimental conditions including these first three factors were held constant, but factors such as the degree of localization must have evolved and likely contributed to the changing frictional behavior in the shale. Whether the relation between surface anisotropy and frictional behavior we observed also holds at larger displacements and when other factors are varied remains to be tested. However, the close correspondence between the sign of $a\text{-}b$ and the anisotropy in the shale faults suggests that the surface roughness anisotropy can be used as an indication of the ability to nucleate unstable slip on a fault.

MECHANISM: ELONGATING ASPERITIES

Our results show that the change in frictional behavior toward velocity-strengthening slip is due to the impact of the evolving roughness on the friction parameter b. The data show that b, not a, controlled $a\text{-}b$ for our tested materials (Fig. 2F), including a strong decrease in b coinciding with the striation development in the shale, an effect also observed with increasing

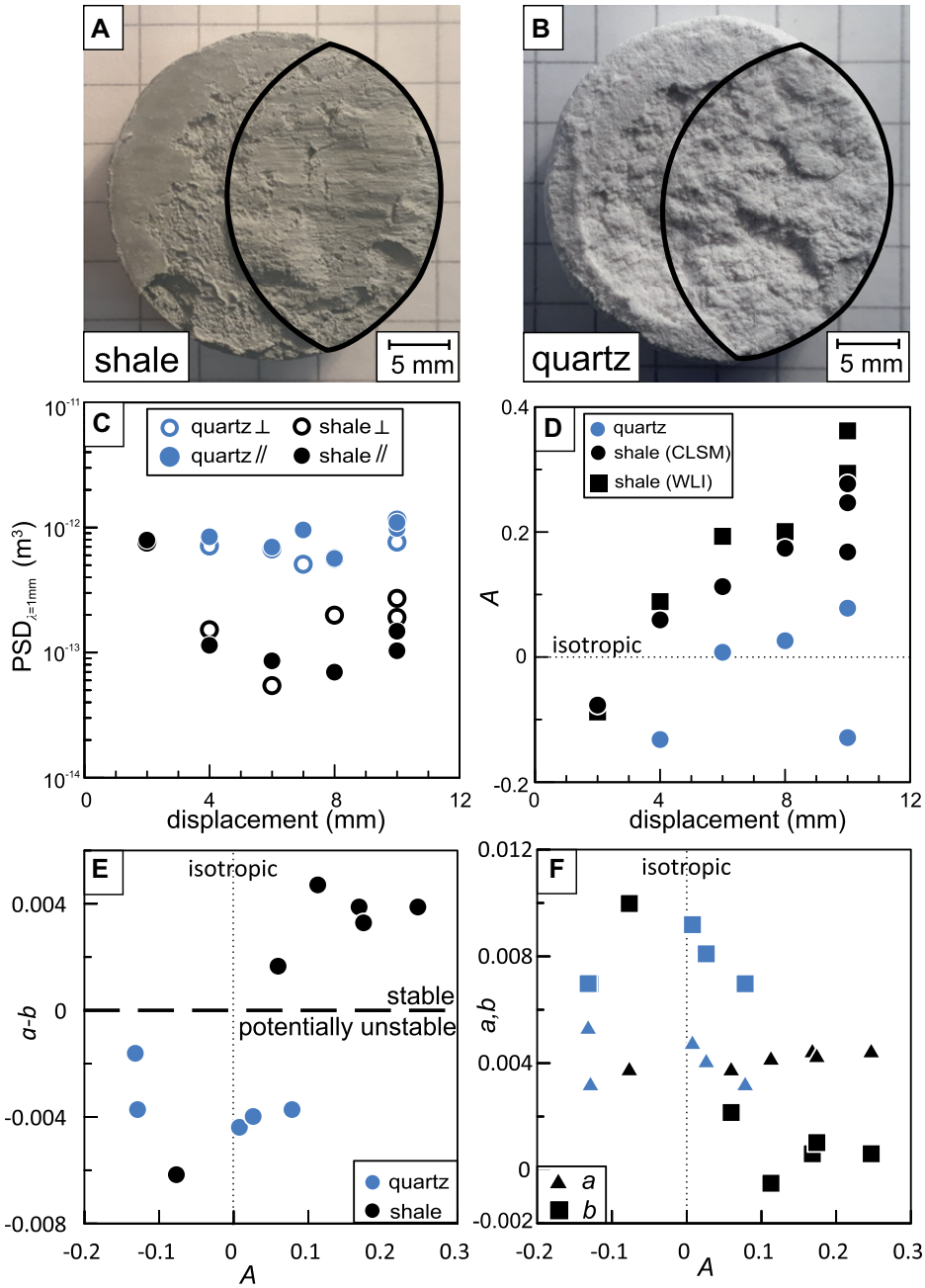

Figure 2. Fault roughness development with displacement. (A,B) Visible striations parallel to the sliding direction (horizontal) develop in shale (A), but not in quartz (B), after 10 mm displacement. (C) Roughness (power spectral density [PSD]) at a wavelength (λ) of 1 mm. (D) Anisotropy, *A*. (E) Frictional stability parameter (*a*-*b*). (F) Individual friction parameters *a* and *b*. CLSM—confocal laser scanning microscope; WLI— white light interferometer; ⊥ indicates perpendicular; || indicates parallel.

slip on salt crystals (Voisin et al., 2007). Micromechanical studies of friction suggest that the rate-dependent friction parameter b is related to the rate at which real contact areas grow with time, for contacts across an interface or between grains within a finite-thickness shear zone (Dieterich and Kilgore, 1994). The small values of b observed for shale are consistent with elongation and flattening of contact asperities during slip, which mechanically increases the contact surface area, reducing the local contact stress and thus limiting the asperity growth rate.

We propose that the geometric evolution of the experimental fault surfaces reflects this physical change in the contact asperities, which would also be applicable to grain-grain contacts within a distributed slip zone. Figures 3A–3C show that the topographical highs, which presumably act as contact asperities, become elongated with slip on the shale fault surfaces, whereas the topographical highs on the quartz faults do not become elongated after 10 mm of slip. Even when the total real area of contact (approximated by the sizes of the colored regions in Figures 3A–3C) is the same for the different anisotropy values, the asperities on the anisotropic surfaces are longer in the slip direction.

We infer that the development of larger, more elongated contact areas is therefore the mechanism promoting velocity-strengthening friction and stable slip in our shale samples. This is likely due to the relatively low hardness of the clay grains in the shale compared to quartz (Deirieh et al., 2012), which results in larger contact areas under the same normal load (Pei et al., 2005), combined with the platy shape and intrinsically low interparticle friction of illite grains (Saffer and Marone, 2003), which facilitate rearrangement of grains into grooves (Fagereng and Ikari, 2020).

IMPLICATIONS FOR NATURAL FAULTS

The fault surfaces that developed during our laboratory experiments exhibit the same power-law scaling of roughness with length scales as is observed over several length scales for natural faults, with similar scaling exponents; i.e., $H < 1$ (Power et al., 1987; Candela et al., 2012). Extrapolation of experimental work to complex natural faults is notoriously difficult, but these similarities suggest that it should be possible to relate our measurements of frictional parameters, especially a, b, and a-b, to the features and inferred processes that operate on natural fault surfaces, at the scales of asperities that are relevant for earthquake nucleation.

Relating the critical slip distance, D_c, to a physical quantity measurable on faults is not as straightforward due to the well-known discrepancy between laboratory-measured values of several to tens of micrometers and values of meters inferred for earthquakes (Scholz, 1998; Kanamori and Brodsky, 2004). D_c has traditionally been associated with asperity size (Dieterich and Kilgore, 1994), suggesting D_c must be scaled from the laboratory to natural faults, since on self-affine surfaces, asperity size depends on the size of the surface area considered. On the other hand, Candela and Brodsky (2016) suggested that D_c might be equivalent to a critical length below which anisotropy is absent, called the minimum scale of anisotropy, L_c. L_c is scale independent, implying that D_c would not have to be scaled. Our results show that D_c is in the range 80–120 μm and L_c is ~20 μm for the shale, and D_c is ~20 μm and L_c is ~200 μm for the quartz (Fig. S6). These values are sufficiently similar that a link should be considered, but L_c is generally outside of the range of measured D_c values. Therefore, we cannot conclusively determine if $L_c = D_c$ and if D_c must be scaled from the laboratory to the field.

We emphasize that although our results suggest that an anisotropic fault surface will prevent earthquake nucleation, it will not necessarily prevent the propagation of coseismic slip from

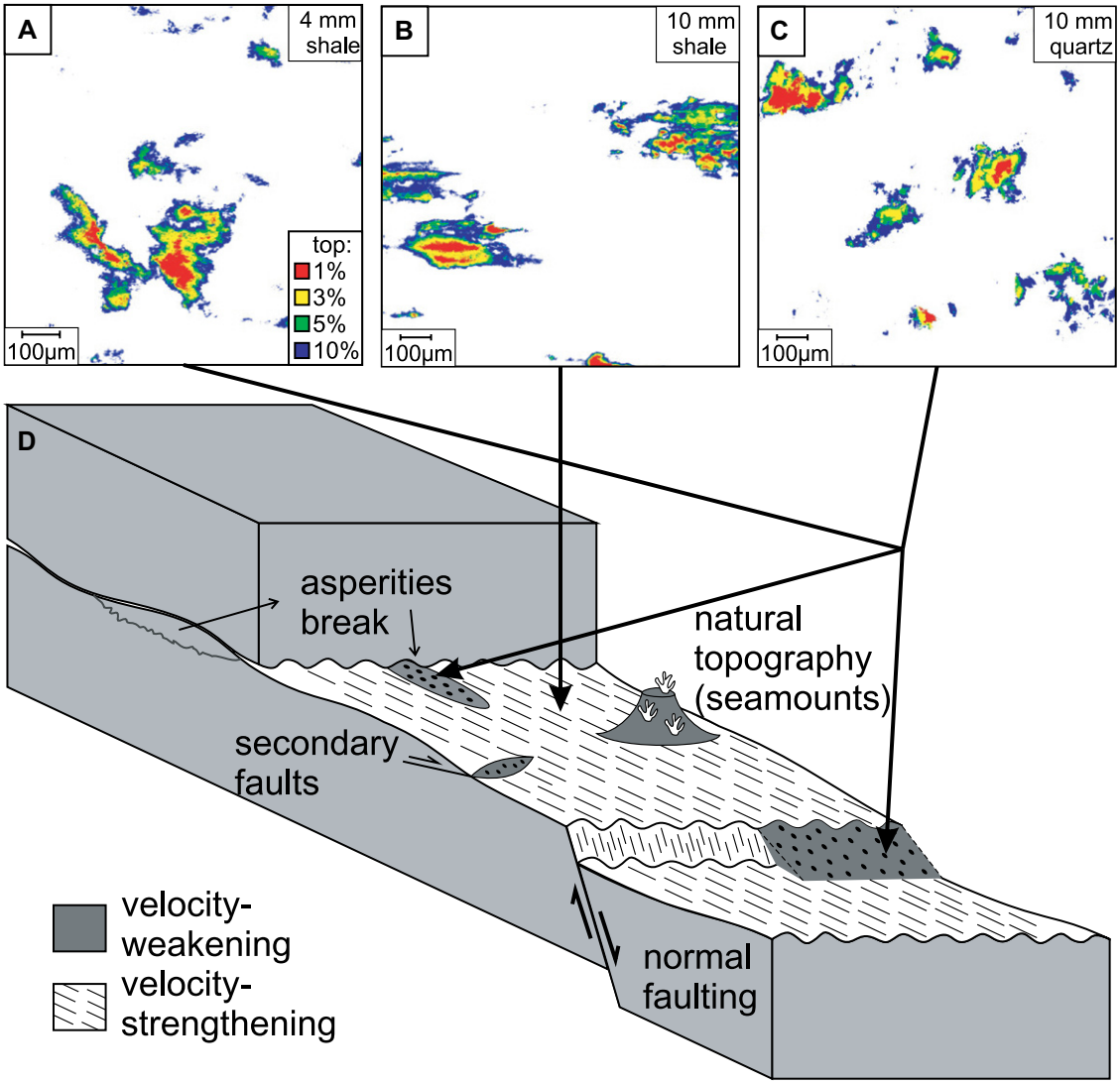

Figure 3. (A–C) Size/shape of contact asperities for actual contact areas of 1%, 3%, 5%, or 10%, showing (A) isotropic roughness for shale surfaces after 4 mm of displacement, (B) anisotropic and elongated asperities in shale after 10 mm of shear displacement, and (C) isotropic roughness in quartz after 10 mm of displacement. (D) On natural faults, various processes can cause rough, anisotropic patches.

other, remote areas of the fault. Most measurements of natural fault surfaces (Renard et al., 2006; Sagy et al., 2007; Bistacchi et al., 2011) show $H_{\parallel} < H_{\perp}$, even though some of these faults are known to have slipped coseismically (Bistacchi et al., 2011). For some of these faults, dynamically propagating slip may have either formed the striations themselves or forced a striated fault patch to slip coseismically. This is, however, out of the scope of our study since our experiments were conducted at subseismic sliding velocities and are relevant for earthquake nucleation only.

The formation of a smooth, striated, velocity-strengthening fault surface is also not necessarily permanent; fault surface roughness may be modified by re-roughening processes (e.g., grain plucking, intersection with secondary faults, healing and refracture, asperity break-off; Fig. 3D). Re-roughening processes have been documented over a wide range of scales, from plucking of micrometer-scale grains (Shervais and Kirkpatrick, 2016) to the kilometer-scale interaction of secondary faults (Kirkpatrick et al., 2020), showing the potential of our relation. Re-roughening at length scales relevant to earthquake nucleation on otherwise striated, velocity-strengthening faults may be a mechanism for creating velocity-weakening fault patches, enabling repeated earthquakes. Furthermore, if anisotropy at the scale of asperities relevant to earthquake nucleation can be inferred from anisotropy at larger length scales that may be observable remotely, then the fractal nature of fault roughness may be leveraged to provide an indication of earthquake nucleation potential at the outcrop scale.

Finally, we emphasize that the relation between sliding stability and roughness does not have to be limited to faults. For example, the rate-and-state friction framework used in this study has been successfully used to describe the motion of landslides (Lacroix et al., 2020) and glaciers (Zoet et al., 2020). Striations have been observed in terrestrial (Shuzui, 2001) and submarine landslides (Gee et al., 2005), in debris avalanches generated by volcanic flank collapse (Hughes et al., 2020), and in glacier bedrocks (Kamb, 1970). Systematic roughness measurements of natural landslide slip surfaces and glacier basal surfaces would be needed to determine whether they display the same self-affine scalable roughness as fault surfaces, and if this roughness correlates with frictional behavior in a similar manner.

ACKNOWLEDGMENTS

This research was supported by European Research Council (ERC) starting grant 714430 (PREDATORS) to M.J. Ikari, Natural Sciences and Engineering Research Council of Canada Discovery Grant RGPIN-2016–04677 to J.D. Kirkpatrick, and ERC Advanced grant 101019628 to F. Renard. We thank the reviewers for their detailed comments, which helped us to improve the manuscript significantly.

REFERENCES CITED

Badt, N., Hatzor, Y.H., Toussaint, R., and Sagy, A., 2016, Geometrical evolution of interlocked rough slip surfaces: The role of normal stress: Earth and Planetary Science Letters, v. 443, p. 153–161, https://doi.org/10.1016/j.epsl.2016.03.026.

Biegel, R.L., Wang, W., Scholz, C.H., Boitnott, G.N., and Yoshioka, N., 1992, Micromechanics of rock

friction: 1. Effects of surface roughness on initial friction and slip hardening in Westerly granite: Journal of Geophysical Research, v. 97, p. 8951–8964, https://doi.org/10.1029/92JB00042.

Bistacchi, A., Ashley Griffith, W., Smith, S.A.F., di Toro, G., Jones, R., and Nielsen, S., 2011, Fault roughness at seismogenic depths from LIDAR and photogrammetric analysis: Pure and Applied Geophysics, v. 168, p. 2345–2363, https://doi.org/10.1007/s00024-011-0301-7.

Brodsky, E.E., Kirkpatrick, J.D., and Candela, T., 2016, Constraints from fault roughness on the scale-dependent strength of rocks: Geology, v. 44, p. 19–22, https://doi.org/10.1130/G37206.1.

Candela, T., and Brodsky, E.E., 2016, The minimum scale of grooving on faults: Geology, v. 44, p. 603–606, https://doi.org/10.1130/G37934.1.

Candela, T., Renard, F., Klinger, Y., Mair, K., Schmittbuhl, J., and Brodsky, E.E., 2012, Roughness of fault surfaces over nine decades of length scales: Journal of Geophysical Research: Solid Earth, v. 117, B08409, https://doi.org/10.1029/2011JB009041.

Collettini, C., Niemeijer, A., Viti, C., and Marone, C., 2009, Fault zone fabric and fault weakness: Nature, v. 462, p. 907–910, https://doi.org/10.1038/nature08585.

Deirieh, A., Ortega, J.A., Ulm, F.J., and Abousleiman, Y., 2012, Nanochemomechanical assessment of shale: A coupled WDS-indentation analysis: Acta Geotechnica, v. 7, p. 271–295, https://doi.org/10.1007/s11440-012-0185-4.

den Hartog, S.A.M., and Spiers, C.J., 2014, A microphysical model for fault gouge friction applied to subduction megathrusts: Journal of Geophysical Research: Solid Earth, v. 119, p. 1510–1529, https://doi.org/10.1002/2013JB010580.

Dieterich, J.H., and Kilgore, B.D., 1994, Direct observation of frictional contacts: New insights for state-dependent properties: Pure and Applied Geophysics, v. 143, p. 283–302, https://doi.org/10.1007/BF00874332.

Doblas, M., 1998, Slickenside kinematic indicators: Tectonophysics, v. 295, p. 187–197, https://doi.org/10.1016/S0040-1951(98)00120-6.

Fagereng, Å., and Ikari, M.J., 2020, Low-temperature frictional characteristics of chlorite-epidote-amphibole assemblages: Implications for strength and seismic style of retrograde fault zones: Journal of Geophysical Research: Solid Earth, v. 125, p. e2020JB019487, https://doi.org/10.1029/2020JB019487.

Gee, M.J.R., Gawthorpe, R.L., and Friedmann, J.S., 2005, Giant striations at the base of a submarine landslide: Marine Geology, v. 214, p. 287–294, https://doi.org/10.1016/j.margeo.2004.09.003.

Harbord, C.W.A., Nielsen, S.B., De Paola, N., and Holdsworth, R.E., 2017, Earthquake nucleation on rough faults: Geology, v. 45, p. 931–934, https://doi.org/10.1130/G39181.1.

Hughes, A., Kendrick, J.E., Salas, G., Wallace, P.A., Legros, F., Di Toro, G., and Lavallée, Y., 2020, Shear localisation, strain partitioning and frictional melting in a debris avalanche generated by volcanic flank collapse: Journal of Structural Geology, v. 140, https://doi.org/10.1016/j.jsg.2020.104132.

Kamb, B., 1970, Sliding motion of glaciers: Theory and observation: Reviews of Geophysics, v. 8, p. 673–728, https://doi.org/10.1029/RG008i004p00673.

Kanamori, H., and Brodsky, E.E., 2004, The physics of earthquakes: Reports on Progress in Physics, v. 67, p. 1429–1496, https://doi.org/10.1088/0034-4885/67/8/R03.

Kirkpatrick, J.D., Edwards, J.H., Verdecchia, A., Kluesner, J.W., Harrington, R.M., and Silver, E.A., 2020, Subduction megathrust heterogeneity characterized from 3D seismic data: Nature Geoscience, v. 13, p. 369–374, https://doi.org/10.1038/s41561-020-0562-9.

Lacroix, P., Handwerger, A.L., and Bièvre, G., 2020, Life and death of slow-moving landslides: Nature Reviews: Earth & Environment, v. 1, p. 404–419, https://doi.org/10.1038/s43017-020-0072-8.

Logan, J.M., and Rauenzahn, K.A., 1987, Frictional dependence of gouge mixtures of quartz and montmorillonite on velocity, composition and fabric: Tectonophysics, v. 144, p. 87–108, https://doi.org/10.1016/0040-1951(87)90010-2.

Okubo, P.G., and Dieterich, J.H., 1984, Effects of physical fault properties on frictional instabilities produced on simulated faults: Journal of Geophysical Research, v. 89, p. 5817–5827, https://doi.org/10.1029/JB089iB07p05817.

Pei, L., Hyun, S., Molinari, J.F., and Robbins, M.O., 2005, Finite element modeling of elasto-plastic contact between rough surfaces: Journal of the Mechanics and Physics of Solids, v. 53, p. 2385–2409, https://doi.org/10.1016/j.jmps.2005.06.008.

Power, W.L., Tullis, T.E., Brown, S.R., Boitnott, G.N., and Scholz, C.H., 1987, Roughness of natural fault surfaces: Geophysical Research Letters, v. 14, p. 29–32, https://doi.org/10.1029/GL014i001p00029.

Renard, F., Voisin, C., Marsan, D., and Schmittbuhl, J., 2006, High resolution 3D laser scanner measurements of a strike-slip fault quantify its morphological anisotropy at all scales: Geophysical Research Letters, v. 33, L04305, https://doi.org/10.1029/2005GL025038.

Saffer, D.M., and Marone, C., 2003, Comparison of smectite- and illite-rich gouge frictional properties: Application to the updip limit of the seismogenic zone along subduction megathrusts: Earth and Planetary Science Letters, v. 215, p. 219–235, https://doi.org/10.1016/S0012-821X(03)00424-2.

Sagy, A., Brodsky, E.E., and Axen, G.J., 2007, Evolution of fault-surface roughness with slip: Geology, v. 35, p. 283–286, https://doi.org/10.1130/G23235A.1.

Sagy, A., Tesei, T., and Collettini, C., 2017, Fault-surface geometry controlled by faulting mechanisms: Experimental observations in limestone faults: Geology, v. 45, p. 851–854, https://doi.org/10.1130/G39076.1.

Scholz, C.H., 1998, Earthquakes and friction laws: Nature, v. 391, p. 37–42, https://doi.org/10.1038/34097.

Shervais, K.A.H., and Kirkpatrick, J.D., 2016, Smoothing and re-roughening processes: The geometric evolution of a single fault zone: Journal of Structural Geology, v. 91, p. 130–143, https://doi.org/10.1016/j.jsg.2016.09.004.

Shuzui, H., 2001, Process of slip-surface development and formation of slip-surface clay in landslides in Tertiary volcanic rocks, Japan: Engineering Geology, v. 61, p. 199–220, https://doi.org/10.1016/S0013-7952(01)00025-4.

Tesei, T., Carpenter, B.M., Giorgetti, C., Scuderi, M.M., Sagy, A., Scarlato, P., and Collettini, C., 2017, Friction and scale-dependent deformation processes of large experimental carbonate faults: Journal of Structural Geology, v. 100, p. 12–23, https://doi.org/10.1016/j.jsg.2017.05.008.

Toy, V.G., Niemeijer, A.R., Renard, F., Morales, L., and Wirth, R., 2017, Striation and slickenline development on quartz fault surfaces at crustal conditions: Origin and effect on friction: Journal of Geophysical Research: Solid Earth, v. 122, p. 3497–3512, https://doi.org/10.1002/2016JB013498.

Voisin, C., Renard, F., and Grasso, J.R., 2007, Long term friction: From stick-slip to stable sliding: Geophysical Research Letters, v. 34, L13301, https://doi.org/10.1029/2007GL029715.

Wallace, L.M., Saffer, D.M., Barnes, P.M., Pecher, I.A., Petronotis, K.E., LeVay, L.J., and the Expedition 372/375 Scientists, 2019, Hikurangi Subduction Margin Coring, Logging and Observatories: Proceedings of the International Ocean Discovery Program Volume 372B/375: College Station, Texas, International Ocean Discovery Program, https://doi.org/10.14379/iodp.proc.372B375.2019.

Zoet, L.K., Ikari, M.J., Alley, R.B., Marone, C., Anandakrishnan, S., Carpenter, B.M., and Scuderi, M.M., 2020, Application of constitutive friction laws to glacier seismicity: Geophysical Research Letters, v. 47, p. e2020GL088964, https://doi.org/10.1029/2020GL088964.

Printed in USA